EPJ D
Atomic, Molecular, Optical and Plasma Physics
EPJ.org
your physics journal

Eur. Phys. J. D (2015) 69: 242 DOI: 10.1140/epjd/e2015-60256-7

Interaction of a two-dimensional electromagnetic pulse with an electron inhomogeneity in an array of carbon nanotubes in the presence of field inhomogeneity

Alexander V. Zhukov, Roland Bouffanais, Hervé Leblond, Dumitru Mihalache, Eduard G. Fedorov and Mikhail B. Belonenko

edp sciences
Società Italiana di Fisica
Springer

Eur. Phys. J. D (2015) 69: 242
DOI: 10.1140/epjd/e2015-60256-7

THE EUROPEAN PHYSICAL JOURNAL D

Regular Article

Interaction of a two-dimensional electromagnetic pulse with an electron inhomogeneity in an array of carbon nanotubes in the presence of field inhomogeneity

Alexander V. Zhukov[1,a], Roland Bouffanais[1], Hervé Leblond[2], Dumitru Mihalache[3,4], Eduard G. Fedorov[5,6], and Mikhail B. Belonenko[7,8]

[1] Singapore University of Technology & Design, 8 Somapah Road, 487372 Singapore
[2] LUNAM Université, Université d'Angers, Laboratoire de Photonique d'Angers, EA 4464, 2 boulevard Lavoisier, 49000 Angers, France
[3] Academy of Romanian Scientists, 54 Splaiul Independentei, 050094 Bucharest, Romania
[4] Horia Hulubei National Institute of Physics and Nuclear Engineering, 077125 Magurele, Romania
[5] Scientific and Industrial Corporation "Vavilov State Optical Institute", 199034 Saint Petersburg, Russia
[6] ITMO University, 197191 Saint Petersburg, Russia
[7] Laboratory of Nanotechnology, Volgograd Institute of Business, 400048 Volgograd, Russia
[8] Volgograd State University, 400062 Volgograd, Russia

Received 27 April 2015 / Received in final form 25 August 2015
Published online 3 November 2015 –

Abstract. In this study, we address the challenging problem of propagation of infrared electromagnetic two-dimensional bipolar pulses of extremely short duration in a heterogeneous array of semiconductor carbon nanotubes. Heterogeneity is defined here as a region of high electron density. The evolutions of the electromagnetic field and charge density in the sample are described by Maxwell's equations and the continuity equation respectively, wherein the inhomogeneity of the field along the nanotube axis is integrated and incorporated into the modeling framework. Our numerical solution to this problem shows the possibility of a stable propagation of two-dimensional electromagnetic pulses through a heterogeneous array of carbon nanotubes. This propagation of electromagnetic pulses is accompanied by a redistribution of the electron density in the sample. For the first time to the best of our knowledge, this latter effect is fully accounted for in our study. Specifically, we demonstrate that depending on the initial speed of the electromagnetic pulse two possible outcomes might ensue: either (i) the pulse overcomes the region of increased electron concentration, or alternatively (ii) it is reflected therefrom. As a result, a near-infrared pulse is transmitted, while the long-wavelength infrared pulse is reflected, on an obstacle that is much smaller than its wavelength.

1 Introduction

One of the most promising objects for modern nanoelectronics is the ensemble of carbon nanotubes (CNTs) [1,2], which represent quasi-one-dimensional macromolecules of carbon. The nonlinearity of the electron dispersion in nanotubes leads to a wide range of properties, which manifest in fields of moderate intensity $\sim 10^3$–10^5 V/cm (see, e.g., Refs. [3,4] and references therein). Recent successes in laser-based optical physics in the generation of powerful electromagnetic radiations with given parameters [5], have provided the impetus for comprehensive studies of electronic and optical properties of CNTs in the presence of an electromagnetic field. Special interest in phenomena related to the propagation of ultrashort electromagnetic pulses through an array of CNTs [6–11] has recently been mounting. In particular, the possibility for propagation of solitary electromagnetic waves in an array of CNTs has been demonstrated [6,7], as well as the dynamics of a periodic train of electromagnetic pulses, and the induced current domains have been investigated [8,9].

Generally, the theoretical and experimental studies of electromagnetic solitary waves have a rather long history. In the last decade, the researches on the morphogenesis of localized structures in optics and photonics and in related areas, such as Bose-Einstein condensates, have attracted a growing body of interest (see Refs. [12–22] and references therein for thorough reviews on these topics). More generally, the study of propagation of stable/quasistable ultrashort optical solitons with duration of only a few cycles requires approaches beyond the standard slowly varying envelope approximation and specific types of medium

[a] e-mail: alex_zhukov@sutd.edu.sg

nonlinearity, see for example the recent overviews [23–26]. The control of medium nonlinearity and of the corresponding features of the electromagnetic wave propagation can be performed, e.g., by a proper choice of nonlinear optical lattices (a topic comprehensively reviewed in Ref. [14]). In this context, the CNT arrays provide one of the unique and practically reliable systems for studying various aspects of electromagnetic wave propagation in nonlinear media. Earlier studies of the propagation of electromagnetic pulses in CNTs were mainly devoted to the analysis of one-dimensional (1D) cases. Later on it was realized that there are a lot of unsolved remaining issues in two-dimensional (2D) and three-dimensional (3D) cases, some of which are quite peculiar. Indeed, the possibility of propagation of cylindrically symmetric electromagnetic waves in an array of nanotubes has been demonstrated [27]. Furthermore, the possibility of propagation of 2D traveling solitary electromagnetic waves (a.k.a. *light bullets*) has been reported in reference [28] (see also Ref. [29]). Subsequently, their interaction with inhomogeneities in the arrays of nanotubes has been investigated [30–32]. The possibility of propagation of 2D bipolar electromagnetic pulses in semiconductor arrays of CNTs was revealed in reference [33]. The general aspects of stability of the laser beams propagating in an array of CNTs were analyzed in reference [34].

It should be noted that the theoretical analysis in the abovementioned studies has been performed under the assumption of homogeneity of the pulse field along the axis of the CNTs. However, the heterogeneity of this field can cause the emergence of interesting and unexpected physical effects of potential practical importance. In particular, reference [35] is concerned with the 2D model of the propagation of ultrashort electromagnetic pulses in an array of CNTs with the heterogeneity of the field along their axis. Furthermore, a comprehensive study of the latter problem in the fully 3D case was recently carried out, which resulted in the demonstration of the possibility of 3D bipolar electromagnetic breather propagation through an array of CNTs with account for the field inhomogeneity [36]. As a result, it was found that in that specific case, an electromagnetic pulse induces a significant redistribution of the electron density in the sample, both in 2D and 3D systems.

Apart from the field inhomogeneity leading to the electrons redistribution, there are other natural heterogeneities in the experimental samples. A case of special importance is when heterogeneities are caused by regions of increased conduction electron concentration, induced by the presence of impurities. In this regard, it seems appropriate to study the effects of heterogeneity of the electron concentration on the characteristics of propagation of extremely short bipolar electromagnetic pulses through an array of semiconducting carbon nanotubes. Note that a similar, yet highly simplified model was previously considered in reference [37], where the electron heterogeneity has been considered in the form of a step-function and the field inhomogeneity has been ignored. The key conceptual advances of the present study are as follows: (i) account for the inhomogeneity of electric field along the CNTs axes, and (ii) account for the heterogeneity due to the electron density distribution.

The paper is constructed as follows. The effective equation describing the evolution of the electric field during the propagation of two-dimensional extremely short bipolar electromagnetic pulses through an inhomogeneous array of semiconductor CNTs is derived in Section 2. In Section 3, we describe the choice of initial conditions used to derive the solution of the problem. In Section 4, we present the outcome of numerical simulations and we thoroughly discuss the obtained results. The main conclusions of our study are summarized in Section 5. In Appendix we give the details of the numerical methods used in this work.

2 General formulation of the problem

2.1 General provisions

Let us consider the propagation of a solitary electromagnetic wave (infrared laser pulse) through a volumetric array of a monolayer of semiconductor carbon nanotubes of the zigzag type, $(m, 0)$, where the number m (not a multiple of three) determines the radius of the nanotube through $R = m\sqrt{3}b/2\pi$, with b the distance between nearest-neighbor carbon atoms [4]. The nanotubes are supposed to be placed into a homogeneous insulator in a way that the axes of the nanotubes are parallel to the common Ox-axis, and the distances between neighboring nanotubes are large compared to their diameter, which allows us to neglect the interaction between CNTs [33,34].

Given the above framework, the dispersion relation for the conduction electrons of CNTs takes the form

$$\gamma(p_x, s) = \gamma_0 \left\{ 1 + 4\cos\left(p_x \frac{d_x}{\hbar}\right)\cos\left(\pi\frac{s}{m}\right) + 4\cos^2\left(\pi\frac{s}{m}\right)\right\}^{1/2}, \quad (1)$$

where the quasimomentum is given by $\mathbf{p} = \{p_x, s\}$, s being the number characterizing the momentum quantization along the perimeter of the nanotube, $s = 1, 2, \ldots, m$, γ_0 being the overlap integral and $d_x = 3b/2$ [3,4].

Assume that the laser pulse propagates perpendicular to the nanotubes axes (along the Oz-axis of a Cartesian coordinate system), the associated electric field $\mathbf{E} = (E, 0, 0)$ being oriented along the Ox axis. The characteristic length over which noticeable changes occur in the pulse field along the Oy-axis is supposed to be substantially greater than the size of the array of nanotubes in the direction of this axis. The later assumption allows us to assume a field to be quasi-uniform along the Oy direction, so that we can justify a two-dimensional model of the system in the xOz-plane. We also suppose that the characteristic pulse duration T_S satisfies the condition $T_S \ll t_{\mathrm{rel}}$, where t_{rel} is the characteristic relaxation time. This condition allows us to use the collisionless approximation in the present study [6].

Let us bear in mind that the pulse field inhomogeneity along the nanotubes axis can lead to a redistribution of the concentration of conduction electrons in the sample and the appearance of regions with low and high charge density. Thus, we assume that the electrons in an array of nanotubes are subjected to the influence of an electromagnetic field associated with a vector potential, $\mathbf{A}$, and a scalar potential, φ. The electromagnetic field in an array of nanotubes will therefore be described by Maxwell's equations [38,39] for the vector and scalar potentials of the field in the system.

2.2 Equations for the field potentials

Maxwell's equations with the Lorentz gauge condition [38,39],

$$\nabla\mathbf{A}+\frac{\varepsilon}{c}\frac{\partial\varphi}{\partial t}=0, \tag{2}$$

lead us to the following equation for the vector potential:

$$\frac{\varepsilon}{c^2}\frac{\partial^2\mathbf{A}}{\partial t^2}-\nabla^2\mathbf{A}-\frac{4\pi}{c}\mathbf{j}=0, \tag{3}$$

where $\mathbf{A}=\{A,0\}$ is the vector potential, $\mathbf{j}=\{j,0\}$ is the current density, ε is the dielectric constant of the medium, and c is the speed of light in vacuum. Hereinafter, the notations for the vector projections are written in the plane $\{x,z\}$. The electric field is classically related to the field potentials via [38,39]

$$\mathbf{E}=-\frac{1}{c}\frac{\partial\mathbf{A}}{\partial t}-\nabla\varphi. \tag{4}$$

We define the conduction current density in the array of carbon nanotubes using the approach developed in references [33,34,36]. Specifically, we represent the electron energy spectrum (1) as a Fourier series, and then write the expression for the projection of the current density on the Ox-axis in the collisionless approximation as

$$j=-en\frac{d_x}{\hbar}\gamma_0\sum_{s=1}^{m}\sum_{r=1}^{\infty}G_{r,s}\sin\left\{r\frac{d_x}{\hbar}\left(A\frac{e}{c}+e\int_0^t\frac{\partial\varphi}{\partial x}dt\right)\right\}, \tag{5}$$

where e is the electron charge, n is the concentration of conduction electrons in the array of nanotubes, and the coefficients $G_{r,s}$ are explicitly given by

$$G_{r,s}=-r\frac{\delta_{r,s}}{\gamma_0}\frac{\int_{-\pi}^{\pi}\cos(r\alpha)\exp\left\{-\sum_{r=1}^{\infty}\theta_{r,s}\cos r\alpha\right\}d\alpha}{\sum_{s=1}^{m}\int_{-\pi}^{\pi}\exp\left\{-\sum_{r=1}^{\infty}\theta_{r,s}\cos(r\alpha)\right\}d\alpha}, \tag{6}$$

with $\theta_{r,s}=\delta_{r,s}(k_BT)^{-1}$, T stands for the temperature, k_B is the Boltzmann constant, and $\delta_{r,s}$ are the coefficients in the expansion of the spectrum (1) in a Fourier series:

$$\delta_{r,s}=\frac{d_x}{\pi\hbar}\int_{-\pi\hbar/d_x}^{\pi\hbar/d_x}\gamma(p_x,s)\cos\left(r\frac{d_x}{\hbar}p_x\right)dp_x. \tag{7}$$

We emphasize, that the value of the conduction electrons concentration in the expression (5) is generally a function of both position and time, i.e., $n=n(x,z,t)$.

The equation governing the evolution of the vector potential field in the array of nanotubes follows from the combination of equations (3) and (5). Direct substitution gives

$$\frac{\partial^2\Psi}{\partial\tau^2}-\left(\frac{\partial^2\Psi}{\partial\xi^2}+\frac{\partial^2\Psi}{\partial\zeta^2}\right)+\eta(\xi,\zeta,\tau)\sum_{s=1}^{m}\sum_{r=1}^{\infty}G_{r,s}\sin\left\{r\left(\Psi+\int_0^{\tau}\frac{\partial\Phi}{\partial\xi}d\tau\right)\right\}=0, \tag{8}$$

where $\eta=\eta(\xi,\zeta,\tau)=n(\xi,\zeta,\tau)/n_0$ is the dimensionless electron concentration, n_0 is the equilibrium electron concentration in a homogeneous specimen in the absence of electromagnetic field, $\Psi=A\frac{ed_x}{c\hbar}$ is the projection of dimensionless vector potential onto the Ox-axis, $\Phi=\varphi\frac{ed_x}{c\hbar}\sqrt{\varepsilon}$ is the dimensionless scalar potential, $\tau=\omega_0t/\sqrt{\varepsilon}$ is the dimensionless time, $\xi=x\omega_0/c$ and $\zeta=z\omega_0/c$ are the dimensionless coordinates, and ω_0 is the frequency determined through

$$\omega_0=2\frac{|e|d_x}{\hbar}\sqrt{\pi\gamma_0n_0}. \tag{9}$$

The redistribution of the electron density distribution is accompanied by a change in the scalar potential field in the system. Maxwell's equations [38,39] give the equation governing the evolution of the dimensionless scalar potential:

$$\frac{\partial^2\Phi}{\partial\tau^2}-\left(\frac{\partial^2\Phi}{\partial\xi^2}+\frac{\partial^2\Phi}{\partial\zeta^2}\right)=\beta(\eta-1), \tag{10}$$

where $\beta=c\hbar(d_x\gamma_0\sqrt{\varepsilon})^{-1}$.

2.3 Equation for the electron density

The propagation of electromagnetic pulses in the sample leads to fluctuations of the charge density. Inhomogeneity of the field along the Oz-axis, perpendicular to the axis of nanotubes, has no impact on the redistribution of the electron density in the sample, since the interaction between nanotubes is negligible and there is no electric current in the Oz direction. Field inhomogeneity along the Ox-axis causes nonuniformity of the current density along the axis of nanotubes, leading to a redistribution of electron density in the sample. Since the total charge in the sample is conserved, the change in the charge density is determined by the following continuity equation [38]:

$$\frac{\partial j}{\partial x}+e\frac{\partial n}{\partial t}=0. \tag{11}$$

Substituting equation (5) into equation (11), we readily obtain the dimensionless equation determining the evolution of electron concentration due to the influence of the

pulse's electromagnetic field, namely

$$\frac{\partial \eta}{\partial \tau} = \alpha \sum_{s=1}^{m} \sum_{r=1}^{\infty} G_{r,s} \frac{\partial}{\partial \xi} \left\{ \eta \sin \left[r \left(\Psi + \int_0^{\tau} \frac{\partial \Phi}{\partial \xi} d\tau \right) \right] \right\}, \tag{12}$$

where $\alpha = d_x \gamma_0 \sqrt{\varepsilon}/c\hbar$. Thus, the field evolution in our system with account for the redistribution of charge density is determined by the system of equations (8) and (10), supplemented with equation (12).

2.4 Pulse field intensity

The electric field component of an electromagnetic wave propagating along the Oz-axis is directed along the axis of the nanotubes (Ox-axes) by virtue of the transverse nature of electromagnetic waves. Thus, for the electric field component of the electromagnetic waves in an array of nanotubes, we can write $\mathbf{E} = (E(\xi, \zeta, \tau), 0, 0)$. Accounting for equation (4), the electric field projection $E(\xi, \zeta, \tau)$ onto the Ox-axis can be represented through the expression

$$E = E_0 \left(\frac{\partial \Psi}{\partial \tau} + \frac{\partial \Phi}{\partial \xi} \right), \tag{13}$$

where E_0 is defined as

$$E_0 = -\frac{\hbar \omega_0}{e d_x \sqrt{\varepsilon}}. \tag{14}$$

As is well-known, the measured physical quantity is the intensity of the electromagnetic field, which is proportional to the square of the electric field component (see e.g. Ref. [38]), $I = E^2$. Using equations (13) and (14), we easily obtain the following relation

$$I = I_0 \left(\frac{\partial \Psi}{\partial \tau} + \frac{\partial \Phi}{\partial \xi} \right)^2, \tag{15}$$

where $I_0 = E_0^2$ (see Eq. (12)).

3 Initial conditions

3.1 Electron concentration inhomogeneity

Suppose that in an array of carbon nanotubes there is an originally formed region of intense concentration of conduction electrons, which exceeds the concentration n_0 in the rest of the sample volume. Let the region of high electron concentration be a plane layer perpendicular to the Oz-axis with a characteristic *half-thickness* Δz_{imp}, and the size of the layer along the Ox-axis substantially exceeds the characteristic width of the electromagnetic pulse along the axis of the nanotube. We assume that at the initial instance of time, an inhomogeneity of the electron density has the form of a Gaussian distribution [34] and can be modeled by a function of the form

$$\eta(\xi, \zeta, \tau_0) = 1 + \left(\frac{n_{\mathrm{imp}}}{n_0} - 1 \right) \exp \left(-\frac{\zeta^2}{\Delta \zeta_{\mathrm{imp}}^2} \right), \tag{16}$$

where n_{imp} is the maximum electron concentration in the inhomogeneity area, and $\Delta \zeta_{\mathrm{imp}} = \Delta z_{\mathrm{imp}} \omega_0 / c$.

The scalar field potential in the system due to the presence of the layer of increased concentration of electrons (16) at the initial instant of time, can readily be calculated using the Gauss theorem [39]. In dimensionless form, the scalar potential is recast as

$$\Phi(\xi, \zeta, \tau_0) = -\varkappa \Delta \zeta_{\mathrm{imp}}^2 \left\{ \frac{\zeta}{\Delta \zeta_{\mathrm{imp}}} \mathrm{erf} \left(\frac{\zeta}{\Delta \zeta_{\mathrm{imp}}} \right) + \frac{1}{\sqrt{\pi}} \left[\exp \left(-\frac{\zeta^2}{\Delta \zeta_{\mathrm{imp}}} \right) - 1 \right] \right\}, \tag{17}$$

where we introduce the quantity

$$\varkappa = 2\pi^{3/2} \frac{d_x c e^2 n_0}{\omega_0^2 \hbar \sqrt{\varepsilon}} \left(\frac{n_{\mathrm{imp}}}{n_0} - 1 \right).$$

It is worth emphasizing that in equation (17), there is no dependence on the coordinate ξ caused by the presence of a flat layer of increased concentration of electrons at the initial instant in time. Specifically, this electrostatic field is homogeneous along the direction of the nanotube axis (namely the Ox-axis).

3.2 Initial electromagnetic pulse

The choice of the initial form of electromagnetic pulse originates from the following considerations. Equation (8) can be considered as a generalization of the 2D analog of the sine-Gordon equation. The numerical results show that the coefficients (see Eq. (6)) decrease rapidly with increasing r ($|G_{1,s}| \gg |G_{2,s}|$ etc.). Working within a 1D framework and leaving only the first term in the sum over r, equation (8) would lead us to the well known sine-Gordon equation, which admits a classical solution in the form of a breather [40]. Note that the sine-Gordon equation describes, in particular, the evolution of the electromagnetic field in solids (e.g., semiconductor superlattices) and allows for the possibility of propagating bipolar solitary electromagnetic waves in a form of breathers [41]. On this basis, it is logical to assume that the system described by equation (8) leads to the propagation of electromagnetic waves in the form of sine-Gordon breathers. We further assume that the system is irradiated by an electromagnetic pulse, such that at the time $\tau = \tau_0$ its scalar potential field is zero and the "snapshot" of the projection of the dimensionless vector potential field on the Ox-axis has a form similar to the "instantaneous snapshot" of the sine-Gordon equation breather profile, namely:

$$\Psi(\xi, \zeta, \tau_0) = 4\Psi_0 \arctan \left(\frac{\sin \chi}{\cosh \mu} \sqrt{\frac{1}{\Omega^2} - 1} \right) \times \exp \left\{ -\left(\frac{\xi - \xi_0}{\lambda_\xi} \right)^2 \right\}, \tag{18}$$

where the following notations have been used:

$$\chi = \Omega \frac{\tau_0 - (\zeta - \zeta_0)u/v}{\sqrt{1-(u/v)^2}}, \tag{19}$$

$$\mu = \left[\frac{\tau_0 u}{v} - (\zeta - \zeta_0)\right] \sqrt{\frac{1-\Omega^2}{1-(u/v)^2}}, \tag{20}$$

with $\Omega = \omega_B/\omega_0$ being a parameter determined from the frequency of natural field oscillations ω_B ($\Omega < 1$), u being the speed of pulse propagation, $v = c/\sqrt{\varepsilon}$ being the linear speed of electromagnetic waves in the medium, ξ_0 and ζ_0 being the dimensionless coordinates at $\tau = \tau_0$; Ψ_0 is an arbitrary constant that allows us to vary the amplitude of the initial pulse without having to modify u or Ω.

In the expression (18), the first factor represents a "snapshot" of the profile of a breather, propagating with the speed u (see Ref. [40]). The presence of the second factor accounts for the fact that a Gaussian intensity distribution is almost always of interest from a practical point of view in various fields of physics and engineering. Indeed, this is due to the minimum diffraction spreading of Gaussian beams, which at the same time represents a very close approximation to reality: it is simple and yet fully describes the properties of laser radiation [34].

The electric field component of an electromagnetic wave in an array of nanotubes at the initial time $\tau = \tau_0$ has the general form $\mathbf{E} = \{E(\xi, \zeta, \tau_0), 0\}$. The quantity $E(\xi, \zeta, \tau_0)$ can be evaluated in the following way. First, we make the formal substitution $\tau_0 \to \tau$ in equations (19) and (20). As a next step and with the use of equations (18) and (13), we come up with an expression in which we perform the reverse substitution $\tau \to \tau_0$. As a result, we obtain the following expression:

$$E(\xi, \zeta, \tau_0) = 4E_0\Psi_0 \sqrt{\frac{1-\Omega^2}{1-(u/v)^2}} \times \left\{ \frac{\cos\chi \cosh\mu - (u/v)\left(\Omega^{-2}-1\right)^{1/2} \sin\chi \sinh\mu}{\cosh^2\mu + (\Omega^{-2}-1)\sin^2\chi} \right\} \times \exp\left\{ -\left(\frac{\xi - \xi_0}{\lambda_\xi}\right)^2 \right\}, \tag{21}$$

where E_0 is determined from equation (14).

In the long pulse limit (the slowly varying envelope case), equation (14) describes a pulse with a carrier phase χ, and an envelope $\operatorname{sech}\mu$ (given by Eqs. (19) and (20), respectively), according to what the angular frequency should be $\omega_0 = \Omega/\sqrt{1-(u/v)^2}$, and the pulse length should be $\Delta\tau = (v/u)\sqrt{1-(u/v)^2}/\sqrt{1-\Omega^2}$ (the full length at half maximum being then FWHM= $2\ln\left(2+\sqrt{3}\right)\Delta\tau$), in normalized units. The values in physical units are obtained by multiplying the times (and dividing the frequencies) by $\sqrt{\varepsilon}/\omega_0$. Here v/u and u/v are the phase and the group velocities, respectively; they are reciprocal of each other according to the dispersion relation of the approval of the sG equation. However, for the numerical values of parameters we are using, the values of the ratio FWHM/T_0 between the pulse width and the optical period $T_0 = 2\pi/\omega_0$ ranges from 0.5 to 0.24. In this sub-cycle range, the quantities evaluated in the long pulse limit appreciably differ from the actual ones. The central angular frequency ω of the pulse can be evaluated by numerically computing the Fourier transform $\hat{E}(\omega)$ of the field given by equation (14), and then computing the mean value

$$\omega_c = \frac{\int_{-\infty}^{\infty} \omega |\hat{E}(\omega)|^2 d\omega}{\int_{-\infty}^{\infty} |\hat{E}(\omega)|^2 d\omega}.$$

The pulse length can be evaluated according to the $D4\sigma$ standard, with

$$\sigma^2 = \frac{\int_{-\infty}^{\infty} |E^2| t^2 dt}{\int_{-\infty}^{\infty} |E^2| dt}$$

for a pulse centered at $t = 0$, then FWHM= $2\sqrt{2\ln 2}\sigma$.

In summary, the initial conditions for the potentials of the electromagnetic field in the system at the initial time $\tau = \tau_0$ have been chosen based on the forms reported in references [34,35]. The scalar potential (see Eq. (17)) determines the electrostatic field generated by the enhanced electron density initially given by equation (16), while the vector potential (see Eq. (18)) determines the electric field of the electromagnetic pulse initially given by equation (21).

4 Numerical simulation and discussion of results

4.1 Choice of parameters

The system of equations, (8), (10) and (12), has no exact analytical solution in the general case, therefore we have numerically studied the propagation of an electromagnetic pulse in an array of carbon nanotubes. To solve this set of governing equations (Eqs. (8), (10), and (12)), with initial conditions (16)–(21), we applied an explicit difference scheme [42] (see details in Appendix). Thus, as a result, we evaluated the quantities $\Psi = \Psi(\xi, \zeta, \tau)$ and $\Phi = \Phi(\xi, \zeta, \tau)$, giving us the field and the associated intensity through the formulas (13) and (15), respectively. It is worth adding that with our analysis we also have access to the dynamics of the modified dimensionless distribution of the quantity $\eta = \eta(\xi, \zeta, \tau)$, thereby allowing us to compute the concentration of electrons in the sample, $n = n_0\eta$.

In our numerical simulations, we have used the following realistic parameters of the medium: $m = 7$, $b = 1.42 \times 10^{-8}$ cm, $\gamma_0 = 2.7$ eV, $d_x \approx 2.13 \times 10^{-8}$ cm, $n_0 = 2 \times 10^{18}$ cm^{-3}, $T = 77$ K, $\varepsilon = 4$, $\omega_0 \approx 10^{14}$ s^{-1} (see Eq. (9) and Refs. [36,37]). Suppose that in the array of nanotubes we have a layer formed by the enhanced electron concentration $n_{\text{imp}} = 30n_0$ with a characteristic width $\Delta z_{\text{imp}} = 3 \times 10^{-5}$ cm that corresponds to a dimensionless width $\Delta\zeta \approx 0.1$. As stated above, we use the collisionless approximation in the present study, which is justified when considering processes at times t

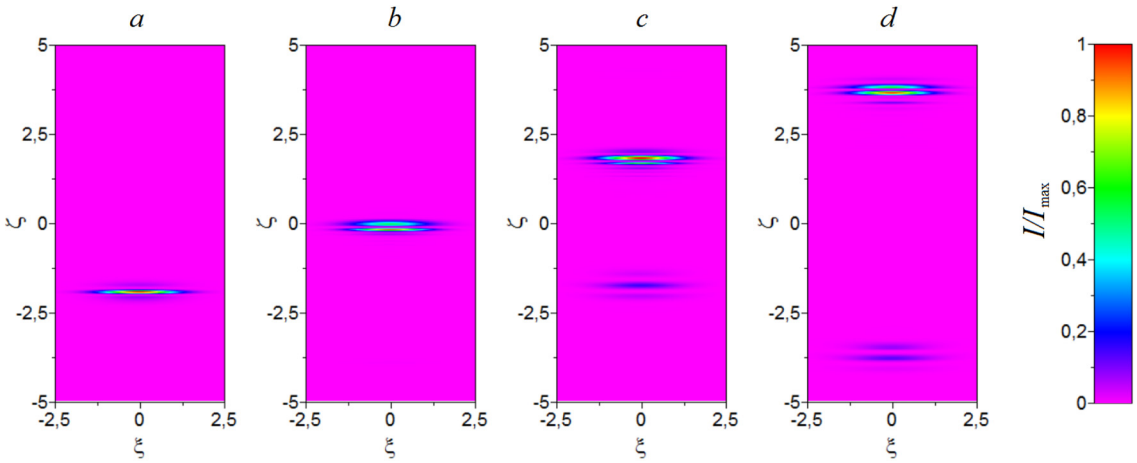

Fig. 1. Intensity distribution of the pulse field in an array of CNTs (while passing through the heterogeneous layer) with $u/v = 0.997$, $\lambda = 2.49$ μm, at different instants of the dimensionless time τ: (a) $\tau = 0$, (b) $\tau = 2.0$, (c) $\tau = 4.0$, (d) $\tau = 6.0$. The axes are scaled using the dimensionless coordinates $\xi = x\omega_0/c$, and $\zeta = z\omega_0/c$. The values of the ratio $I/I_{\max}$ are mapped on a color scale, the maximum values of the field intensity correspond to red, and minimum ones to purple. $I_{\max}$ is the maximum value of I at the given instant τ considered.

not exceeding the relaxation time $t_{\rm rel} \approx 3 \times 10^{-13}$ s (see Refs. [3,4]). With the parameters chosen above it means $\tau_{\rm rel} = \omega_0 t/\sqrt{\varepsilon} \approx 15$. The relative initial pulse velocity, u/v, was varied in a range between 0.500 and 0.999. In the particular range $u/v < 0.5$, the problem has no practical interest since the pulse travels too short a distance during a time $\tau_{\rm rel}$, which is comparable with its own halfwidth. On the other hand, we do not consider the range $u/v > 0.999$ because of limitations associated with the specifics of the selected numerical scheme (see Appendix). The parameter Ω – being proportional to the natural oscillations frequency – has being varied in a range between 0.3 and 0.7. In the case when $\Omega < 0.3$, the electromagnetic pulse becomes too narrow and a fundamental change in its shape has not been observed with decreasing value down below 0.5. On the other hand, increasing Ω beyond 0.7 yields a pulse that is too wide in the $O\zeta$ direction, which makes its halfwidth comparable to the size of our numerical domain. The parameter λ_ξ – the halfwidth of the pulse along the $O\xi$-axis – has been varied between 0.5 and 1.5, though we did not observe any qualitative differences in the pulse behavior and dynamics. The parameter Ψ_0 has been varied between 0.05 and 1. When chosen above all other values of the system parameters, there are realistic – in terms of possible experiments – initial values of the peak amplitude of the electric field pulse if the value of Ψ_0 is within the specified limits. In particular, for $u/v = 0.997$ the peak amplitude of the electric field is $E_p = 4E_0\Psi_0(1-\Omega^2)^{1/2}(1-(u/v)^2)^{-1/2} \approx 7.0\times10^6$ V/cm, while for $u/v = 0.95$ we have $E_p \approx 1.7 \times 10^6$ V/cm (see Eq. (21)).

For definiteness, we have chosen the following initial values for the laser pulse parameters: $\Omega = 0.5$, which corresponds to the natural mode frequency $\omega_B = \Omega\omega_0 \approx 5.05 \times 10^{13}$ s^{-1}; $\lambda_\xi = 1$, which corresponds to the actual halfwidth along the Ox-axis being $L_x = \lambda_\xi c/\omega_0 \approx 3 \times 10^{-4}$ cm; $\Psi_0 = 0.1$, $\xi_0 = 0$, and $\tau = \tau_0$.

Computing the wavelength in vacuum $\lambda = 2\pi c\sqrt{\varepsilon}/(\omega_0\omega_c)$ with these parameters, it is seen that it ranges from near infrared ($\lambda = 1.43$ μm for a normalized velocity $u/v = 0.999$), to far infrared ($\lambda = 43$ μm for $u/v = 0.5$). The corresponding FWHM ranges from 2.82 to 100 fs, and the number of cycles within the pulse, i.e., the ratio between the FWHM and the optical period T, is about 0.6 for all considered values (0.7 for $u/v = 0.5$). Hence, the input pulses are a bit longer than half-cycle.

4.2 Results of the simulations

As mentioned earlier, our numerical analysis considered the $0.5 < u/v < 0.999$ range, which covers a wide part of the infrared domain, 43 μm $< \lambda <$ 1.43 μm. However, within that range, our results revealed that the most interesting physical phenomena where concentrated in the much narrower region $0.95 \le u/v \le 0.997$ (i.e., 10.4 μm $< \lambda <$ 2.49 μm), as is shown below. Figures 1–4 represent typical results of the current study of the propagation of laser pulses through an inhomogeneous array of CNTs with account for a realistic and dynamic field distribution.

First, let us consider the upper bound case $u/v = 0.997$, $\lambda = 2.49$ μm. Our numerical results show that the interaction between the ultrashort bipolar laser pulse with the electron inhomogeneity is strongly dependent on the initial speed of the pulse speed u, which can naturally be expected from equation (18). Figures 1 and 2 represent a passage of the electromagnetic pulse propagating with initial velocity $u = 1.496 \times 10^{10}$ cm/s, corresponding to $u/v = 0.997$ (see Eq. (16)), i.e., a subcycle pulse with central wavelength in vacuum $\lambda < 2.49$ μm), and pulse duration FWHM = 4.9 fs, through the region of enhanced electron concentration. Figure 1 reveals the temporal evolution of the distribution of field intensity $I(\xi, \zeta, \tau)$ when

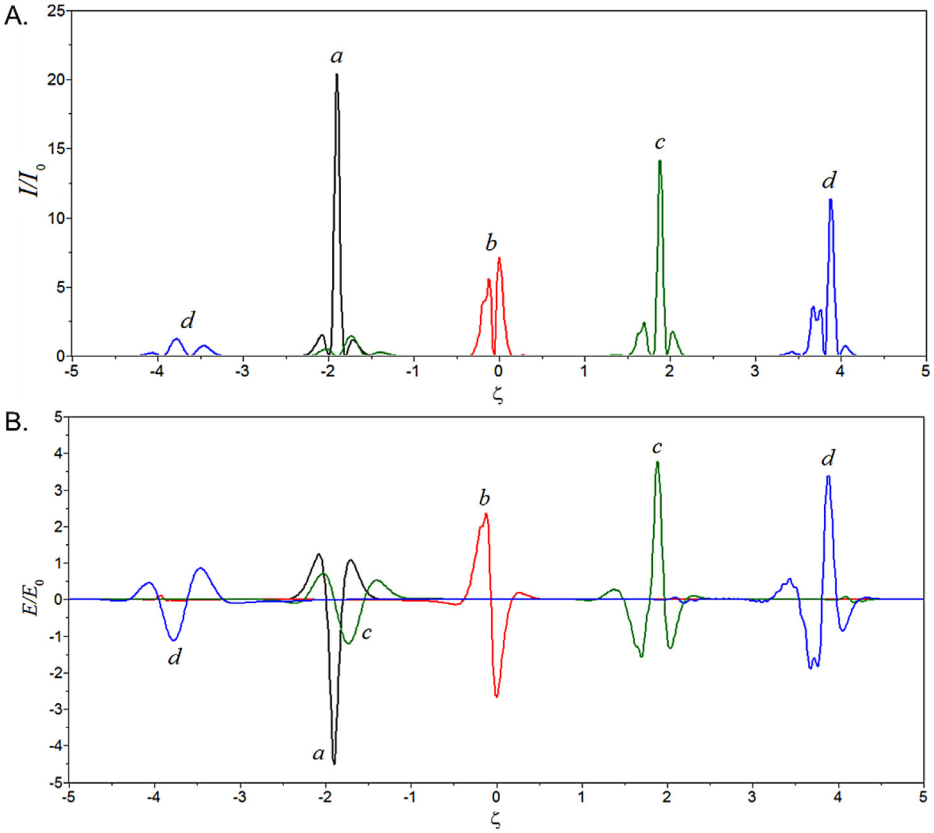

Fig. 2. A: Intensity distribution $I(\xi_0, \zeta, \tau)/I_{\max}$ of the pulse field in an array of CNTs with $u/v = 0.997$, $\lambda = 2.49$ μm in an area parallel to the $\nu O\zeta$-plane and passing through the point with $\xi = \xi_0$, at different instants of the dimensionless times: (a) $\tau = 0$, (b) $\tau = 2.0$, (c) $\tau = 4.0$, (d) $\tau = 6.0$. B: The same for the electric field amplitude.

considering four different instants separated by the dimensionless duration $\tau^* = \omega_0 t^*/\sqrt{\varepsilon} = 2$. The field intensity is represented through the ratio $I/I_{\max}$, different values of which correspond to a variation of colors (flooded contours) with a colormap from violet to red. The quantity $I_{\max}$ is the maximum value of intensity at that given instant in time. Red areas correspond to near-maximum intensity, while violet ones reflect near-minimum intensity regions. With the above chosen parameters, unit values along the axes $O\xi$ and $O\zeta$ correspond to the real physical distances $\sim 3 \times 10^{-4}$ cm, and hence the propagation is shown over a distance of about 30 μm.

To supplement our two-dimensional analysis in the $\xi O\zeta$-plane shown in Figure 1, we further consider one-dimensional lines corresponding to constant values for ξ. Figure 2 shows the profile of the field intensity $I(\xi_0, \zeta, \tau)$ along the $O\zeta$-line, in a plane parallel to the $\nu O\zeta$-plane, with the pulse passing trough the point $\xi = \xi_0$ (the center of the pulse is along the $O\xi$-axis) at the same instants as those considered in Figure 1. Figure 2 reveals a typical change in the shape of the laser pulsing maximum value of intensity $I_{\max}$ during a passage through the region of enhanced electron density. In general, as can be seen from Figures 1 and 2, a 2D bipolar electromagnetic pulse, after interaction with the inhomogeneous layer, continues to steadily propagate along the initial direction with insignificant dispersal spreading. Hence, the short-wavelength infrared pulse is almost integrally transmitted.

As a next step, we turn our attention to the lower bound case $u/v = 0.95$, $\lambda = 10.4$ μm. of the narrower range of interesting values for this problem. Figures 3 and 4 are concerned with the interaction of a laser pulse with the region of enhanced electron density for an initial value of the pulse velocity $u = 1.425 \times 10^{10}$ cm/s (i.e. $u/v = 0.95$, which corresponds to a wavelength in vacuum $\lambda = 10.4$ μm, and a pulse duration FWHM$\simeq$ 20 fs). Figure 3 shows the temporal evolution of the distribution of field intensity $I(\xi, \zeta, \tau)$ when considering four different instants separated by the dimensionless duration $\tau^* = \omega_0 t^*/\sqrt{\varepsilon} = 2$, similarly to what has been done previously. The profile of the field intensity $I(\xi_0, \zeta, \tau)$ along the $O\zeta$-line is shown in Figure 4, in a plane parallel to the $\nu O\zeta$-plane, with the pulse passing trough the point $\xi = \xi_0$ (the center of the pulse is along the $O\xi$-axis) at the same instants as those considered in Figure 3.

Interestingly, we observe that if the initial pulse has an insufficient initial velocity, then it is unable to overcome the area of inhomogeneous electron distribution, though it continues to propagate stably, but in the opposite direction. Thus, the results of our numerical analysis reveal that the dynamics of interaction of the laser pulse with a layer of increased concentration of electrons crucially

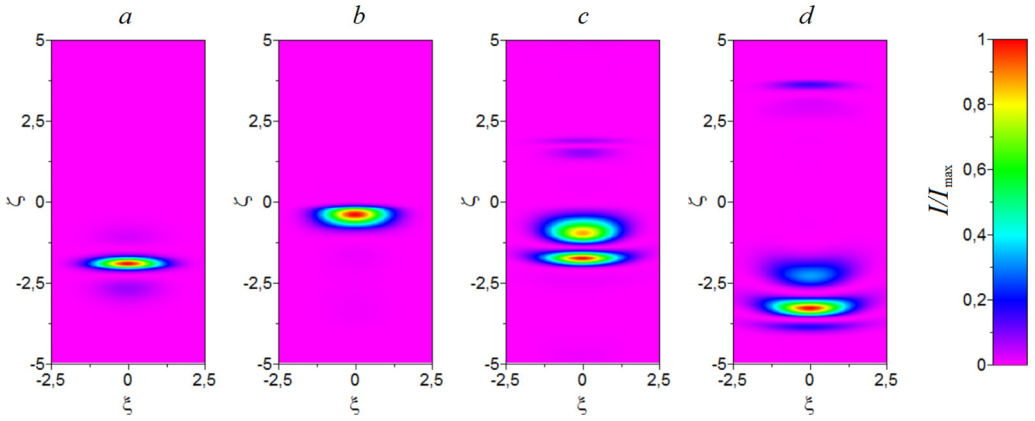

Fig. 3. Intensity distribution of the pulse field in an array of CNTs (while reflecting from heterogeneous region) with $u/v = 0.95$, $\lambda = 10.4$ μm at different instants of the dimensionless time τ: (a) $\tau = 0$, (b) $\tau = 2.0$, (c) $\tau = 4.0$, (d) $\tau = 6.0$. The axes are scaled using the dimensionless coordinates $\xi = x\omega_0/c$, and $\zeta = z\omega_0/c$. Values of the ratio $I/I_{\max}$ are mapped on a color scale, the maximum values of the field intensity correspond to red, and minimum ones to purple. $I_{\max}$ is the maximum value of I at the given instant τ considered.

depends on the initial velocity of the pulse. Electromagnetic pulses with low propagation velocities are reflected from a region of enhanced electron density, while pulses with velocities exceeding a certain threshold value u_c are able to overcome the region of high electron density. The value of u_c depends on several factors, which include the heterogeneity parameters: the ratio of the electron concentration n_{imp}/n_0, as well as the characteristic width of the inhomogeneity layer $2\Delta z_{\text{imp}}$.

We have to emphasize that our results are completely consistent with the earlier simplified model considered in reference [37]. The principal difference lies in the account for the realistic inhomogeneity as well as the inhomogeneity of the field along the nanotubes axis. This allowed us to solve the problem self-consistently with full account of the realistic and dynamic redistribution of the electrons. As stated in reference [37], this principal result is consistent with earlier investigations of different systems. For instance, in the study reported in reference [41], the authors demonstrated the selective nature of the transmission of electromagnetic solitons through the region of high electron density in quantum semiconductor superlattices.

We can therefore conclude that an array of semiconducting carbon nanotubes acts as a "filter" for extremely short electromagnetic pulses, which selectively transmits pulses with parameters satisfying certain conditions – in the particular of our study, for pulses with $u > u_c$. This interesting effect, in our opinion, may serve as the basis for manufacturing optical logic elements and laser radiation control devices. It results in the reflection of almost all energy of the input long wavelength infrared pulse, on a very short obstacle. Recall indeed that the size of the inhomogeneity layer (full length at $1/e$) is $2\Delta z_{\text{imp}} = 0.6$ μm, almost one order of magnitude below the linear wavelength in the medium, $\lambda/\sqrt{\varepsilon} \simeq 5$ μm.

It is worth adding that the inhomogeneity of the field distribution along the nanotubes axis as included in our model, does not violate the conclusion on the stability of propagation of extremely short pulses. The main difference as compared with our previous study [37] consists in the shape of the electromagnetic pulses. Indeed, within the frame of homogeneous field consideration [37], the shape of the tail – notice the "ripples" of small amplitude – appearing behind the propagating pulse is due to the imbalance between competing nonlinear and dispersive effects. In the present study, we incorporate an additional important factor, namely the dynamic redistribution of electrons associated with the field inhomogeneity.

Another way to analyze the nature of the interaction of ultrashort pulses with an area of increased concentration of electrons can be achieved by studying the coefficients of transmission K_T and reflection K_R defined as follows:

$$K_T = \frac{\int_0^{+\infty} d\zeta \int_{-\infty}^{+\infty} I(\xi,\zeta)d\xi}{\int_{-\infty}^{+\infty} \int_{-\infty}^{+\infty} I(\xi,\zeta)d\zeta d\xi}, \tag{22}$$

$$K_R = \frac{\int_{-\infty}^{0} d\zeta \int_{-\infty}^{+\infty} I(\xi,\zeta)d\xi}{\int_{-\infty}^{+\infty} \int_{-\infty}^{+\infty} I(\xi,\zeta)d\zeta d\xi}. \tag{23}$$

The system considered in this paper – owing to the choice of a model that assumes the collisionless approximation – is conservative. A direct consequence of the energy conservation is the following simple relation between K_T and K_R:

$$K_T + K_R = 1, \tag{24}$$

which is verified by our numerical analysis as shown in Figure 5. Let us explain the physical meaning of the variables defined by equations (22) and (23). By definition, K_T (resp. K_R) is the ratio of the energy of the wave-packet that has overcome the region (resp. that is reflected therefrom) of the area of increased concentration of electrons to the total energy of the initial wave-packet.

Figure 5 shows the dependence of the reflection and transmission coefficients the initial pulse velocity u/v (at time $\tau = \tau_0 = 0$). Our numerical analysis shows that with increasing values of u/v, there is an increase in the

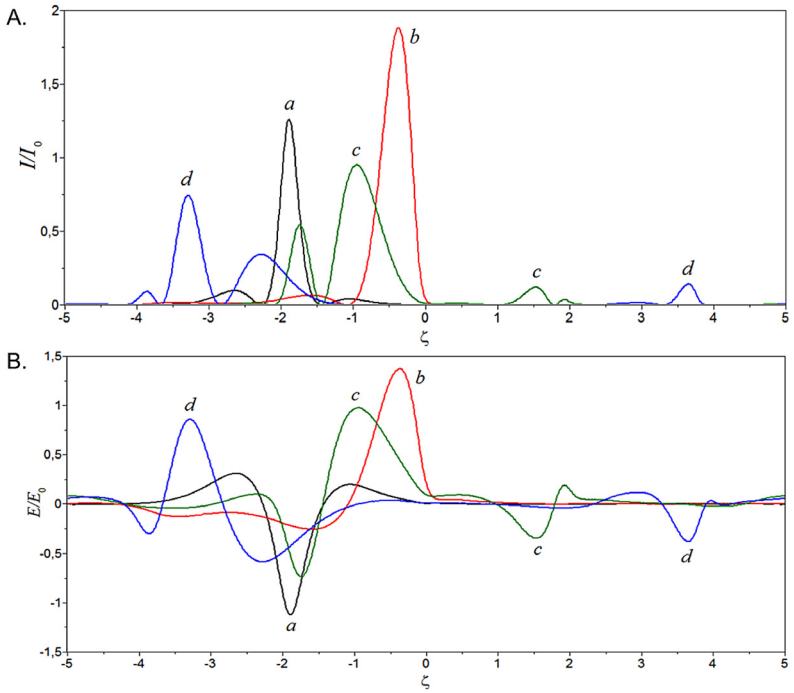

Fig. 4. A: Intensity distribution $I(\xi_0, \zeta, \tau)/I_{\max}$ of the pulse field in an array of CNTs with $u/v = 0.95$, $\lambda = 10.4$ μm, in an area parallel to the $\nu O\zeta$-plane and passing through the point with $\xi = \xi_0$ (but reflecting from heterogeneous region), at different instants of the dimensionless times: (a) $\tau = 0$, (b) $\tau = 2.0$, (c) $\tau = 4.0$, (d) $\tau = 6.0$. B: The same for the electric field amplitude.

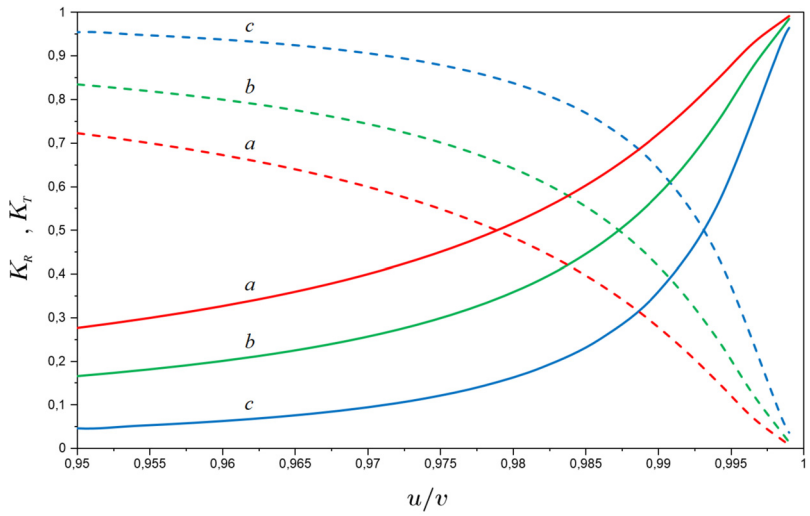

Fig. 5. Variations of the reflection coefficient K_R (dashed lines) and transmission coefficient K_T (solid curves) with the initial pulse speed for different values of the inhomogeneity of the electron density n_{imp}/n_0: (a) $n_{\text{imp}}/n_0 = 15$ (red curves); (b) $n_{\text{imp}}/n_0 = 20$ (green curves); (c) $n_{\text{imp}}/n_0 = 30$ (blue curves).

transmission coefficient (solid curves) with, of course, a concomitant decrease – as a result of equation (24) – in the reflection one (dashed curves). The initial speed of the pulse at which there is equality between the transmission and reflection coefficients, can be considered as the critical speed ratio $(u/v)_c$ defined by the condition $K_T\left((u/v)_c\right) = K_R\left((u/v)_c\right)$. In other words, when the pulse speed exceeds this critical speed, u_c, the component of the pulse transmitted through the region of increased concentration of electrons is larger that its reflected component.

From Figure 5 we see that the graphs for $K_T(u/v)$ and $K_R(u/v)$ intersect at the point corresponding to their value $K_T = K_R = 0.5$. For different values of the inhomogeneity parameter n_{imp}/n_0 and Δz_{imp}, this equality remains true for different values of the critical velocity ratio $(u/v)_c$. In particular, $(u/v)_c$ increases with increasing values of the parameter n_{imp}/n_0. Our analysis

shows that varying the latter parameter as $n_{\rm imp}/n_0 = 15, 20, 30$, the critical velocity ratio changes as $(u/v)_c = 0.978, 0.988, 0.993$, so that the dependence of $(u/v)_c$ with respect to $n_{\rm imp}/n_0$ is clearly nonlinear. The critical values of the velocity ratio correspond to critical values of the wavelength 6.80 μm, 5.00 μm, and 3.81 μm, respectively. A more detailed study of the dependence of the critical speed with the various parameters of heterogeneity will be provided in a future study of the more general case of the interaction of light pulses in a three-dimensional model.

As already hinted earlier, the results of the present study might open new possibilities for the practical development of innovative nanoelectronic devices. Indeed, the peculiar features of propagation of extremely short electromagnetic pulses in a heterogeneous array of semiconducting carbon nanotubes could potentially be used in the development of new devices for field control of the laser radiation, optical information processing systems, as well as for nondestructive quality control technologies for systems in nanoelectronics.

5 Conclusions

In summary, the key results of our study are the following:

(i) For the first time to the best of our knowledge, we derived a system of equations describing and governing the evolution of the field and charge density in an array of CNTs in the presence of a region of enhanced electron density, during the propagation of ultrashort electromagnetic pulse with full account of the field inhomogeneity along the nanotubes axis (see Eqs. (8), (10) and (12)).

(ii) It has been established that the interaction with the layer of increased concentration of electrons in the array of nanotubes does not essentially affect the stability of the electromagnetic pulse shape.

(iii) Depending on its initial velocity, the ultrashort laser pulse can either pass through the inhomogeneous region, or get reflected therefrom. The characteristic velocity, corresponding to a passing/reflection turnover, generally depends on the size of the inhomogeneous region as well as the density of electrons in the elevated concentration region.

(iv) Accounting for the field inhomogeneity in this problem leads to a redistribution of electrons in the sample. However, the latter effect only leads to quantitative differences in comparison with the homogeneous case. Qualitatively, the physical phenomenon is essentially unchanged.

The inhomogeneity in a CNT array is thus able to induce a frequency selective reflection, which is almost complete on a very short layer along the propagation axis, much smaller than the wavelength.

Author contribution statement

The contribution of all the authors is equal.

We are grateful to Prof. N.N. Rosanov for valuable discussions and useful recommendations. A.V. Zhukov and R. Bouffanais are financially supported by the SUTD-MIT International Design Centre (IDC). E.G. Fedorov acknowledges partial support from the Foundation for The Support of Leading Universities of the Russian Federation (Grant 074-U01). M.B. Belonenko acknowledges support from the Russian Foundation for Fundamental Research.

Appendix A: Numerical scheme

A.1 Discretization of the system of equations

For the numerical solution of the system of equations (8), (10) and (12), we use the explicit difference three-layer scheme for inhomogeneous equations of hyperbolic type (see, e.g. Ref. [42]). Let us carry out a discretization on the two-dimensional computational grid in $\xi O\zeta$–plane. Spatial coordinates on the grid are defined as follows

$$\xi_i = \left(i - \frac{N_\xi}{2}\right)\Delta\xi, \quad \zeta_k = \left(k - \frac{N_\zeta}{2}\right)\Delta\zeta, \tag{A.1}$$

where i and k are the indices corresponding to grid nodes along the $O\xi$ and $O\zeta$ axes, respectively. It is assumed that $0 \le i \le N_\xi$ and $0 \le k \le N_\zeta$, where N_ξ and N_ζ are the maximum numbers of corresponding nodes; $\Delta\xi$ and $\Delta\zeta$ stand for the grid steps in the respective spatial directions. Let us define the temporal layers through a simple relation $\tau^{(n+1)} = \tau^{(n)} + \Delta\tau$, where $\Delta\tau$ is the time step and n is the number of a given layer.

For the discretization of equations (8), (10) and (12), let us replace the continuous quantities with their discrete counterparts in the following way

$$\begin{aligned}
\Psi(\xi,\zeta,\tau) &\to \Psi(\xi_i,\zeta_k,\tau^{(n)}) \equiv \Psi_{i,k}^{(n)},\\
\Phi(\xi,\zeta,\tau) &\to \Phi(\xi_i,\zeta_k,\tau^{(n)}) \equiv \Phi_{i,k}^{(n)},\\
\eta(\xi,\zeta,\tau) &\to \eta(\xi_i,\zeta_k,\tau^{(n)}) \equiv \eta_{i,k}^{(n)},
\end{aligned} \tag{A.2}$$

$$\eta\sum_{s=1}^{m}\sum_{r=1}^{\infty} G_{r,s}\sin\left\{r\left(\Psi + \int_0^\tau \frac{\partial\Phi}{\partial\xi}d\tau\right)\right\} \to \Lambda_{i,k}^{(n)}, \tag{A.3}$$

$$\alpha\sum_{s=1}^{m}\sum_{r=1}^{\infty} G_{r,s}\frac{\partial}{\partial\xi}\left\{\eta\sin\left[r\left(\Psi + \int_0^\tau \frac{\partial\Phi}{\partial\xi}d\tau\right)\right]\right\} \to \Theta_{i,k}^{(n)}. \tag{A.4}$$

Spatial and temporal derivatives appearing in equations (8), (10) and (12) can be replaced by the following

$$E_{i,k}^{(0)} = 4E_0\Psi_0\sqrt{\frac{1-\Omega^2}{1-(u/v)^2}}\left\{\frac{\cos\chi_k^{(0)}\cosh\mu_k^{(0)} - (u/v)\left(\Omega^{-2}-1\right)^{1/2}\sin\chi_k^{(0)}\sinh\mu_k^{(0)}}{\cosh^2\mu_k^{(0)} + (\Omega^{-2}-1)\sin^2\chi_k^{(0)}}\right\}\exp\left\{-\left(\frac{\xi_k-\xi_0}{\lambda_\xi}\right)^2\right\} \quad \text{(A.16)}$$

finite-difference relations:

$$\frac{\partial^2}{\partial\tau^2}\{\Psi,\Phi\} \to \frac{\{\Psi,\Phi\}_{i,k}^{(n+1)} - 2\{\Psi,\Phi\}_{i,k}^{(n)} + \{\Psi,\Phi\}_{i,k}^{(n-1)}}{\Delta\tau^2},$$
$$\frac{\partial^2}{\partial\xi^2}\{\Psi,\Phi\} \to \frac{\{\Psi,\Phi\}_{i+1,k}^{(n)} - 2\{\Psi,\Phi\}_{i,k}^{(n)} + \{\Psi,\Phi\}_{i-1,k}^{(n)}}{\Delta\tau^2},$$
$$\frac{\partial^2}{\partial\zeta^2}\{\Psi,\Phi\} \to \frac{\{\Psi,\Phi\}_{i,k+1}^{(n)} - 2\{\Psi,\Phi\}_{i,k}^{(n)} + \{\Psi,\Phi\}_{i,k-1}^{(n)}}{\Delta\tau^2}, \quad \text{(A.5)}$$

$$\frac{\partial\eta}{\partial\tau} \to \frac{\eta_{i,k}^{(n+1)} - \eta_{i,k}^{(n)}}{\Delta\tau}. \quad \text{(A.6)}$$

With some straightforward algebra, equations (8), (10) and (12) are recast in the following discrete form

$$\Psi_{i,k}^{(n+1)} = 2\Psi_{i,k}^{(n)} - \Psi_{i,k}^{(n-1)} + \left(\frac{\Delta\tau}{\Delta\xi}\right)^2\left(\Psi_{i+1,k}^{(n)} - 2\Psi_{i,k}^{(n)} + \Psi_{i-1,k}^{(n)}\right) + \left(\frac{\Delta\tau}{\Delta\zeta}\right)^2\left(\Psi_{i,k+1}^{(n)} - 2\Psi_{i,k}^{(n)} + \Psi_{i,k-1}^{(n)}\right) - \Delta\tau^2\Lambda_{i,k}^{(n)}, \quad \text{(A.7)}$$

$$\Phi_{i,k}^{(n+1)} = 2\Phi_{i,k}^{(n)} - \Phi_{i,k}^{(n-1)} + \left(\frac{\Delta\tau}{\Delta\xi}\right)^2\left(\Phi_{i+1,k}^{(n)} - 2\Phi_{i,k}^{(n)} + \Phi_{i-1,k}^{(n)}\right) + \left(\frac{\Delta\tau}{\Delta\zeta}\right)^2\left(\Phi_{i,k+1}^{(n)} - 2\Phi_{i,k}^{(n)} + \Phi_{i,k-1}^{(n)}\right) + \Delta\tau^2\beta\left(\eta_{i,k}^{(n)} - 1\right), \quad \text{(A.8)}$$

$$\eta_{i,k}^{(n+1)} = \eta_{i,k}^{(n)} + \Delta\tau\Theta_{i,k}^{(n)}, \quad \text{(A.9)}$$

$$\Lambda_{i,k}^{(n)} = \eta_{i,k}^{(n)}\sum_{s=1}^{m}\sum_{r=1}^{\infty}G_{r,s}\sin\left\{r\left(\Psi_{i,k}^{(n)} + \mathrm{Int}_{i,k}^{(n)}\right)\right\}, \quad \text{(A.10)}$$

$$\Theta_{i,k}^{(n)} = \frac{\alpha}{2\Delta\xi}\sum_{s=1}^{m}\sum_{r=1}^{\infty}G_{r,s} \times\left\{\eta_{i+1,k}^{(n)}\sin\left[r\left(\Psi_{i+1,k}^{(n)} + \mathrm{Int}_{i+1,k}^{(n)}\right)\right] - \eta_{i-1,k}^{(n)}\sin\left[r\left(\Psi_{i-1,k}^{(n)} + \mathrm{Int}_{i-1,k}^{(n)}\right)\right]\right\}, \quad \text{(A.11)}$$

where $\mathrm{Int}_{i,k}^{(n)}$ stands for a discrete counterpart of the integral $\int_0^\tau d\tau\partial\Phi/\partial\xi$, where we use the simplest two-point difference approximation for the first derivative with respect to ξ. The quantity $\mathrm{Int}_{i,k}^{(n)}$ can be approximated by the recurrent relation

$$\mathrm{Int}_{i,k}^{(n+1)} \approx \mathrm{Int}_{i,k}^{(n)} + \frac{\Delta\tau}{2\Delta\xi}\left(3\Phi_{i+1,k}^{n+1} - 4\Phi_{i,k}^{n+1} + \Phi_{i-1,k}^{n+1}\right), \quad \text{(A.12)}$$

where we have used the three-point difference approximation for the first derivative of $\Phi(\xi,\zeta,\tau)$ with respect to ξ.

Equations (A.7)–(A.9) allow us to compute the values of quantities $\Psi_{i,k}^{(n+1)}$, $\Phi_{i,k}^{(n+1)}$, and $\eta_{i,k}^{(n+1)}$ on an arbitrary $(n+1)$th temporal layer given the prior knowledge of the $(n-1)$th and nth temporal layers.

A.2 Discretization of initial conditions

To solve equations (8), (10) and (12) we have defined the initial conditions given by equations (16)–(18), which have to be used on the zeroth temporal layer, so they must be presented in a discrete form as well. For this purpose, let us complete the following substitutions: $\tau \to \tau^{(0)} = 0$, $\xi \to \xi_i$, $\zeta \to \zeta_k$, $\eta(\xi,\zeta,0) \to \eta_{i,k}^{(0)}$, $\Psi(\xi,\zeta,0) \to \Psi_{i,k}^{(0)}$, $\Phi(\xi,\zeta,0) \to \Phi_{i,k}^{(0)}$, $\chi(\zeta,0) \to \chi_k^{(0)}$, $\mu(\zeta,0) \to \mu_k^{(0)}$. As a result, the initial conditions (16)–(18) read

$$\eta_{i,k}^{(0)} = 1 + \left(\frac{n_{\mathrm{imp}}}{n_0} - 1\right)\exp\left(-\frac{\zeta_k^2}{\Delta\zeta_{\mathrm{imp}}^2}\right), \quad \text{(A.13)}$$

$$\Phi_{i,k}^{(0)} = -\varkappa\Delta\zeta_{\mathrm{imp}}^2\left\{\frac{\zeta_k}{\Delta\zeta_{\mathrm{imp}}}\mathrm{erf}\left(\frac{\zeta_k}{\Delta\zeta_{\mathrm{imp}}}\right) + \frac{1}{\sqrt{\pi}}\left[\exp\left(-\frac{\zeta_k^2}{\Delta\zeta_{\mathrm{imp}}}\right) - 1\right]\right\}, \quad \text{(A.14)}$$

$$\Psi_{i,k}^{(0)} = 4\Psi_0\arctan\left(\frac{\sin\chi_k^{(0)}}{\cosh\mu_k^{(0)}}\sqrt{\frac{1}{\Omega^2}-1}\right) \times\exp\left\{-\left(\frac{\xi_k-\xi_0}{\lambda_\xi}\right)^2\right\}, \quad \text{(A.15)}$$

where

$$\chi_k^{(0)} = -\Omega\left(1-u^2/v^2\right)^{-1/2}(\zeta_k-\zeta_0)u/v$$

and

$$\mu_k^{(0)} = -\left(1-\Omega^2\right)^{1/2}\left(1-u^2/v^2\right)^{-1/2}(\zeta_k-\zeta_0).$$

The discrete counterpart of the expression for the electric part of the wave field (see Eq. (21)) at the initial instant of time, $\tau = 0$, can be presented as $\mathbf{E}_{i,k}^{(0)} = \{E_{i,k}^{(0)}, 0, 0\}$, where

see equation (A.16) *above.*

$$\Psi_{i,k}^{(1)} = \Psi_{i,k}^{(0)} + 4\Delta\tau\Psi_0\sqrt{\frac{1-\Omega^2}{1-(u/v)^2}}\left\{\frac{\cos\chi_k^{(0)}\cosh\mu_k^{(0)} - (u/v)\left(\Omega^{-2}-1\right)^{1/2}\sin\chi_k^{(0)}\sinh\mu_k^{(0)}}{\cosh^2\mu_k^{(0)} + (\Omega^{-2}-1)\sin^2\chi_k^{(0)}}\right\}\exp\left\{-\left(\frac{\xi_k-\xi_0}{\lambda_\xi}\right)^2\right\} \quad \text{(A.19)}$$

A.3 Calculations on the zeroth layer

For convenience, let us number the 0th, 1st, and 2nd layers as $(n-1)$, n, and $(n+1)$, respectively. On the zeroth layer ($\tau^0 = 0$) we have to use the values given explicitly through equations (A.13)–(A.15). The intensity of the wave field is given by $I_{i,k}^{(0)} = (E_{i,k}^{(0)})^2$. Note that the quantity $\mathrm{Int}_{i,k}^{(0)} = 0$ – appearing in equations (A.10) and (A.11) – returns zero on the zeroth layer. This fact will be further used for calculations on the subsequent (first) layer.

A.4 Calculations on the first layer

On the first layer we impose $\tau^{(1)} = \Delta\tau$. It can easily be argued that the scalar potential does not vary considerably on the first layer in comparison with the zeroth one. Furthermore, we assume that $\Phi_{i,k}^{(1)} \approx \Phi_{i,k}^{(0)}$. Strictly speaking, the latter approximation is not quite correct from the mathematical point of view. However, this simplification associated with it does not lead to a significant error in numerical integration for the subsequent temporal layers. The value of the discrete analogue of the dimensionless electron concentration on the first temporal layer $\eta_{i,k}^{(1)}$ can be found from equation (A.9):

$$\eta_{i,k}^{(1)} = \eta_{i,k}^{(0)} + \Delta\tau\Theta_{i,k}^{(0)}. \quad \text{(A.17)}$$

The quantity $\Theta_{i,k}^{(0)}$ in equation (A.17) is obtained from equation (A.11) for $n = 0$, bearing in mind that $\mathrm{Int}_{i,k}^{(0)} = 0$:

$$\Theta_{i,k}^{(0)} = \frac{\alpha}{2\Delta\xi}\sum_{s=1}^{m}\sum_{r=1}^{\infty}G_{r,s}\left\{\eta_{i+1,k}^{(n)}\sin\left[r\Psi_{i+1,k}^{(0)}\right] - \eta_{i-1,k}^{(0)}\sin\left[r\Psi_{i-1,k}^{(0)}\right]\right\}. \quad \text{(A.18)}$$

The quantity $\Psi_{i,k}^{(1)}$ has been computed using the three-point difference approximation for the first time derivative, and the already known value $\Psi_{i,k}^{(0)}$ on the zeroth layer, namely

see equation (A.19) *above.*

The discrete counterpart of the field projection on the nanotubes axis given by equation (13) has been computed using a two-point difference approximation for the first derivatives

$$E_{i,k}^{(1)} = E_0\left(\frac{\Psi_{i,k}^{(1)} - \Psi_{i,k}^{(0)}}{\Delta\tau} + \frac{\Phi_{i+1,k}^{(1)} - \Phi_{i-1,k}^{(0)}}{2\Delta\xi}\right). \quad \text{(A.20)}$$

Calculations on the second temporal layer can be achieved following the exact same scheme, though with $n = 1$. When all the quantities on the first three layers are known, the subsequent layers can be readily treated by the recursion method through a classical iterative process.

A.5 Boundary conditions

Setting up the adequate boundary conditions is of prime importance to achieve a correct implementation of our numerical scheme. During a numerical integration, we vary the number of nodes from 0 to N_ξ (for the $O\xi$-axis) and from 0 to N_ζ (for $O\zeta$-axis), which – on the arbitrary temporal layer n – allows us to evaluate the quantities $\Psi_{i,k}^{(n)}$, $\Phi_{i,k}^{(n)}$, and $\eta_{i,k}^{(n)}$ at every (i,k) node. Note that the right-hand side of equations (7)–(9) contains – in the general case – values of the quantities both on the nodes with $i = k$ and the neighboring nodes with $i, k \pm 1$. A special case appears when the quantities in the left-hand side of the above formulas are at the border of the grid, i.e. when at least one of the equalities $i = 0$, $i = N_\xi$, $k = 0$, or $k = N_\zeta$ applies. In this case, the question arises on how to determine the quantities in the right-hand side term, which are out of the grid border, i.e. on the nodes $i, k-1$ (for $i, k = 0$) or on the nodes $i, k+1$ (for $i, k = N_\xi, N_\zeta$). We have resolved this classical issue in a rather common way (similar to periodic boundary conditions) by "stitching" grid boundaries. Namely the node with indices $i, k = -1$ is believed to be equivalent to the node with indices $i, k = N_\xi, N_\zeta$, and similarly $N_\xi + 1, N_\zeta + 1$ is equivalent to $i, k = 0$. In other words, geometrically speaking our computational grid corresponds to a torus. This geometric interpretation, however, hardly affects the results of our numerical analysis.

References

1. P.J.F. Harris, *Carbon Nanotubes and Related Structures: New Materials for the Twenty-First Century* (Cambridge University Press, 1999)
2. S. Iijima, Nature **354**, 56 (1991)
3. S.A. Maksimenko, G.Ya. Slepyan, J. Commun. Technol. Electron. **47**, 261 (2002)
4. S.A. Maksimenko, G. Ya. Slepyan, *Handbook of Nanotechnology. Nanometer Structure: Theory, Modeling, and Simulation* (SPIE Press, Bellingham, 2004)
5. S.A. Akhmanov, V.A. Vysloukh, A.S. Chirkin, *Optics of Femtosecond Laser Pulses* (AIP, New York, 1992)
6. M.B. Belonenko, E.V. Demushkina, N.G. Lebedev, J. Russ. Laser Res. **27**, 457 (2006)
7. M.B. Belonenko, E.V. Demushkina, N.G. Lebedev, Phys. Solid State **50**, 383 (2008)

8. M.B. Belonenko, E.V. Demushkina, N.G. Lebedev, Technol. Phys. **53**, 817 (2008)
9. M.B. Belonenko, E.V. Demushkina, N.G. Lebedev, Russ. J. Phys. Chem. B **2**, 964 (2008)
10. N.N. Yanyushkina, M.B. Belonenko, N.G. Lebedev, A.V. Zhukov, M. Paliy, Int. J. Mod. Phys. B **25**, 3401 (2011)
11. M.B. Belonenko, A.S. Popov, N.G. Lebedev, A.V. Pak, A.V. Zhukov, Phys. Lett. A **375**, 946 (2011)
12. P. Mandel, M. Tlidi, J. Opt. B **6**, R60 (2004)
13. B.A. Malomed, D. Mihalache, F. Wise, L. Torner, J. Opt. B **7**, R53 (2005)
14. Y.V. Kartashov, B.A. Malomed, L. Torner, Rev. Mod. Phys. **83**, 247 (2011)
15. P. Grelu, N. Akhmediev, Nat. Photon. **6**, 84 (2012)
16. Z. Chen, M. Segev, D. Christodoulides, Rep. Prog. Phys. **75**, 086401 (2012)
17. D. Mihalache, Rom. J. Phys. **57**, 352 (2012)
18. M. Tlidi, K. Staliunas, K. Panajotov, A.G. Vladimirov, M.G. Clerc, Philos. Trans. R. Soc. A **372**, 20140101 (2014)
19. D. Mihalache, Rom. J. Phys. **59**, 295 (2014)
20. B.A. Malomed, J. Opt. Soc. Am. B **31**, 2460 (2014)
21. N.N. Rosanov, G.B. Sochilin, V.D. Vinokura, N.V. Vysotina, Philos. Trans. R. Soc. A **372**, 20140012 (2014)
22. V.S. Bagnato, D.J. Frantzeskakis, P.G. Kevrekidis, B.A. Malomed, D. Mihalache, Rom. Rep. Phys. **67**, 5 (2015)
23. S.V. Sazonov, Bull. Russ. Acad. Sci. Phys. **75**, 157 (2011)
24. H. Leblond, H. Triki, D. Mihalache, Rom. Rep. Phys. **65**, 925 (2013)
25. H. Leblond, D. Mihalache, Phys. Rep. **523**, 61 (2013)
26. D.J. Frantzeskakis, H. Leblond, D. Mihalache, Rom. J. Phys. **59**, 767 (2014)
27. M.B. Belonenko, S. Yu. Glazov, N.G. Lebedev, N.E. Meshcheryakova, Phys. Sol. State **51**, 1758 (2009)
28. M.B. Belonenko, N.G. Lebedev, A.S. Popov, J. Exp. Theor. Phys. Lett. **91**, 461 (2010)
29. H. Leblond, D. Mihalache, Phys. Rev. A **86**, 043832 (2012)
30. M.B. Belonenko, A.S. Popov, N.G. Lebedev, Techn. Phys. Lett. **37**, 119 (2011)
31. A.S. Popov, M.B. Belonenko, N.G. Lebedev, A.V. Zhukov, M. Paliy, Eur. Phys. J. D **65**, 635 (2011)
32. A.S. Popov, M.B. Belonenko, N.G. Lebedev, A.V. Zhukov, T.F. George, Int. J. Theor. Phys. Group Theory Nonlinear Opt. **15**, 5 (2011)
33. E.G. Fedorov, A.V. Zhukov, M.B. Belonenko, T.F. George, Eur. Phys. J. D **66**, 219 (2012)
34. A.V. Zhukov, R. Bouffanais, M.B. Belonenko, E.G. Federov, Mod. Phys. Lett. B **27**, 1350045 (2013)
35. M.B. Belonenko, E.G. Fedorov, Phys. Sol. State **55**, 1238 (2013)
36. A.V. Zhukov, R. Bouffanais, E.G. Fedorov, M.B. Belonenko, J. Appl. Phys. **114**, 143106 (2013)
37. A.V. Zhukov, R. Bouffanais, E.G. Fedorov, M.B. Belonenko, J. Appl. Phys. **115**, 203109 (2014)
38. L.D. Landau, E.M. Lifshitz, L.P. Pitaevskii, *Electrodynamics of Continuous Media*, 2nd edn. (Elsevier, Oxford, 2004)
39. L.D. Landau, E.M. Lifshitz, *The Classical Theory of Fields*, 4th edn. (Butterworth-Heinemann, Oxford, 2000)
40. Yu.S. Kivshar, B.A. Malomed, Rev. Mod. Phys. **61**, 763 (1989)
41. S.V. Kryuchkov, K.A. Popov, Semiconductors **30**, 1130 (1996)
42. J.W. Thomas, *Numerical Partial Differential Equations – Finite Difference Methods* (Springer Verlag, New York, 1995)